

**Equivalent Sensor Radiance Generation and Remote  
Sensing from Model Parameters. Part I: Equivalent Sensor  
Radiance Formulation.**

**G. Wind<sup>1,2</sup>, A. M. da Silva<sup>1</sup>, P.M. Norris<sup>1,3</sup> and S. Platnick<sup>1</sup>**

[1]{NASA Goddard Space Flight Center, 8800 Greenbelt Rd. Greenbelt, Maryland, 20771,  
USA}

[2]{SSAI, Inc. 10210 Greenbelt Road, Suite 600, Lanham, Maryland 20706, USA}

[3]{Universities Space Research Association, 10211 Wincopin Circle # 500, Columbia, MD  
21044, USA}

Correspondence to: G.Wind (Gala.Wind@nasa.gov)

1  
2  
3  
4  
5  
6  
7  
8  
9  
10  
11  
12  
13  
14  
15  
16  
17  
18

## **Abstract**

In this paper we describe a general procedure for calculating equivalent sensor radiances from variables output from a global atmospheric forecast model. In order to take proper account of the discrepancies between model resolution and sensor footprint the algorithm takes explicit account of the model subgrid variability, in particular its description of the probability density function of total water (vapor and cloud condensate.) The equivalent sensor radiances are then substituted into an operational remote sensing algorithm processing chain to produce a variety of remote sensing products that would normally be produced from actual sensor output. This output can then be used for a wide variety of purposes such as model parameter verification, remote sensing algorithm validation, testing of new retrieval methods and future sensor studies. We show a specific implementation using the GEOS-5 model, the MODIS instrument and the MODIS Adaptive Processing System (MODAPS) Data Collection 5.1 operational remote sensing cloud algorithm processing chain (including the cloud mask, cloud top properties and cloud optical and microphysical properties products.) We focus on clouds and cloud/aerosol interactions, because they are very important to model development and improvement.

## 1 Introduction

Accurate knowledge of cloud cover and cloud properties is important in model studies that involve Earth's radiative budget, climate prediction and numerical weather prediction. High clouds are observed to have a net warming effect on the atmosphere because of their low albedo and low temperature. Low clouds have a net cooling effect due to their high albedo and relatively small temperature contrast with the surface. Clouds and their interactions with aerosols are significant sources of uncertainty in climate prediction studies (IPCC, 2007). In addition, clouds continue to be the main source of climate feedback uncertainty and hence climate sensitivity (e.g., Bony et al., 2006).

The Goddard Earth Observing System Version 5 (GEOS-5) earth system model is maintained by the Global Modeling and Assimilation Office (GMAO) at NASA Goddard Space Flight Center (GSFC). GEOS-5 contains components for atmospheric circulation and composition (including atmospheric data assimilation), ocean circulation and biogeochemistry, and land surface processes. Components and individual parameterizations within components are coupled under the Earth System Modeling Framework (ESMF, Hill et al. 2004). In addition to traditional meteorological parameters (winds, temperatures, etc., Rienecker et al. 2008), GEOS-5 includes modules representing the atmospheric composition, most notably aerosols (Colarco et al. 2010) and tropospheric/stratospheric chemical constituents (Pawson et al. 2008), and the impact of these constituents on the radiative processes of the atmosphere. GEOS-5 has a mature atmospheric data assimilation system that builds upon the Grid-point Statistical Interpolation (GSI) algorithm jointly developed with NCEP (Wu et al. 2002, Derber et al. 2003, Rienecker et al. 2008). The GSI solver was originally developed at NCEP as a unified 3D-Var analysis system for supporting global and

1 regional models. GSI includes all the in-situ and remotely sensed data used for operational  
2 weather prediction at NCEP. GEOS-5 also includes assimilation of Aerosol Optical Depth  
3 (AOD) observations from the MODerate resolution Imaging Spectroradiometer (MODIS)  
4 imager on the NASA Earth Observing System (EOS) *Terra* and *Aqua* spacecraft; an  
5 algorithm for assimilating cloud property information from measurements in the visible and  
6 infrared portions of the spectrum is currently under development (Norris and da Silva 2013).  
7 While the GEOS-5 meteorological assimilation includes a wide variety of spaceborne sensor  
8 data, traditionally samples containing clouds are carefully screened out. The near real-time  
9 GEOS-5 data assimilation and forecasting system runs at a nominal horizontal resolution of  
10 25 km with 72 vertical layers (Rienecker et al. 2008, Molod et al. 2012).

11 The MODIS instrument (Barnes et al. 1998) is a passive imager, producing a wide variety  
12 of remotely sensed data products for land, ocean and atmosphere disciplines from 36 spectral  
13 channels. Data Collection 5.1 processing includes algorithms for retrieving cloud cover  
14 amount (Ackerman, et al. 2006, Frey et al. 2008), cloud top properties such as cloud top  
15 pressure and temperature (Menzel et al. 2008) and cloud optical and microphysical properties  
16 such as cloud optical thickness, cloud effective radius and cloud water path (Platnick et al.  
17 2003; Wind et al. 2010; Zhang and Platnick 2011; King et al. 2013).

18 In this paper we present a technique that brings together remote sensing methods and  
19 model-generated fields. We use MODIS geolocation data to sample GEOS-5 fields as if the  
20 MODIS instrument were flying over the model fields instead of the Earth surface. Once the  
21 sampling is complete, we generate equivalent sensor radiance data for the MODIS footprint.  
22 We then replace the contents of the 1 km, 500 m and 250 m resolution MODIS Level-1B  
23 (Xiong, et al. 2006) radiance files with these simulated radiances and insert the resulting  
24 alternate data stream into the start of the MODIS Adaptive Processing System (MODAPS)

1 operational algorithm processing chain for the atmosphere discipline cloud products  
2 mentioned above (product designation MOD06 and MYD06 for Terra and Aqua MODIS,  
3 respectively). The data stream is fully transparent to the system so that pixel-level (Level-2)  
4 retrievals can be aggregated through the same gridded (Level-3)  $1^\circ \times 1^\circ$  code (Hubanks et al.  
5 2006; King et al. 2003, 2013) used in MODAPS production (MOD08 and MYD08 for Terra  
6 and Aqua, respectively). There are many potential uses for the resulting Level-2 and Level-3  
7 data. Level-3 model aggregations can be compared to archived MODIS Level-3 and GEOS-5  
8 source data fields directly as a means of model validation and study of model biases that  
9 could exist. Level-2 data can be used to study some aspects of retrieval algorithm behavior  
10 and sensitivities since all retrievals are performed with known (prescribed) *truth*.

11 The equivalent sensor data framework has been developed with instrument flexibility in  
12 mind, so that by simple substitution of spectral response functions and data reader, the  
13 MODIS instrument can be replaced by other spaceborne or airborne sensors, currently in  
14 operation or part of a future concept, and a different sensor data stream can be produced.  
15 Thus, identical products from different sensors or different retrieval algorithms for the same  
16 sensor can be compared and analyzed in a controlled environment, which can provide insight  
17 and lead to improvements in remote sensing algorithms.

18 This flexibility extends to model data as well. Any climate or weather prediction model  
19 fields can be used as long as a means of ingesting the necessary parameters is provided. Thus  
20 synthetic retrievals based on multiple models can be compared and analyzed using the same  
21 sensor interface in a controlled environment, leading to a consistent diagnostic toolset.  
22 Furthermore, this detailed simulation capability can function as a testbed for very fast  
23 simulators such as the Cloud Feedback Model Intercomparison Project (CFMIP) Observation

1 Simulator Package (COSP) (Bodas-Salcedo, et al. 2011) or the hyperspectral simulator of  
2 Feldman et al. (2011).

3 In section 2 we describe the model–sensor interface using the GEOS-5 model and  
4 MODIS imager. Section 3 shows an example of simulation and retrieval of cloud properties  
5 on a sample Level-2 data granule. In section 4 we elaborate on future directions for the  
6 software suite.

7 This paper is the first part in a series that will combine the software suite described in  
8 detail here with a variety of research applications.

## 9 **2 Radiance simulations at scales smaller than the model's grid spacing**

10 We start the process by selecting an area and time period of study. It can be as small as a  
11 few-pixel subsection of a single MODIS granule or as large as an entire year of MODIS data.  
12 The study size is only limited by availability of computing resources. As far as model itself is  
13 concerned, there is no need for actual MODIS data to be present, but we specifically want the  
14 actual MODIS radiances to be available, so that retrievals from simulated and actual radiances  
15 can be compared directly. Similarities and differences in those retrievals can be analyzed and  
16 results applied on a variety of levels in order to improve both the model and the sensor  
17 retrieval algorithm.

18 For simplicity's sake in all subsequent references and illustrations the study area will be  
19 taken to be a standard 5 minute MODIS data granule (approximate 2000 km in the along track  
20 direction by 2300 km). Once the granule is chosen, we proceed to choose model output files  
21 that bound the granule time. For example, for the granule at 0200 UTC, we would select  
22 model output at 0000 and 0300 UTC. We use a MODIS standard geolocation file (MOD03  
23 product) to define the spatial locations to sample the model fields. Solar and view angle  
24 information contained in the same MODIS geolocation file is also used in the simulation . For

the examples shown in this paper we used the GEOS model v.5.7.2 output. A listing of specific GEOS-5 fields and products used in this suite is given in Table 1.

## 2.1 Surface albedo determination

In order to save on computational time we pre-determine surface albedo for the area of study. The surface albedo data comes from a variety of sources. Over ice-free ocean, MODIS geometry and model wind speed are used in a Cox-Munk ocean surface BRDF model (Cox and Munk, 1954) to produce cloud-free ocean surface reflectance. This model reflectance is calculated for four cardinal wind directions and then averaged into a lookup table (LUT), that is a function of wavelength, wind speed, solar and sensor zenith angles and relative azimuth angle. We do the calculation at three wind speeds of 3, 7 and 15 m/s. The LUT has 33 solar zenith values, 28 view zenith values and 37 relative azimuth values. We linearly interpolate as needed to obtain surface spectral albedo in the selected fifteen MODIS channels that have a shortwave reflective component. The MODIS channels used in the simulation and their central wavelengths are listed in Table 2. The ocean reflectance LUT contains data for channels 1-22 and 26 from the table. For the IR (infrared) channels that have no reflective component (27-36), a constant value of 0.015 is used. This value is based on the ocean surface emissivity value suggested by the MODIS cloud top properties algorithm.

Over land several methods are utilized to model the radiances for all MODIS channels. We use the MODIS land surface spectral albedo gap-filled dataset (Moody et al. 2005, 2008) that has been updated for MODIS data Collection 6 and is derived from both Aqua and Terra data. In addition to providing 16-day time period averages every 8 days, the gap-filled albedo files are generated for each year separately (instead of aggregating all years together as was done previously). Further, spatial resolution has been improved to 1 km. These files are derived from the Collection 5 MCD42B product (C. Schaaf et al., personal communication).

1 This MODIS land surface albedo product is used directly for channels 1-7 and interpolated  
2 linearly to cover other MODIS spectral channels that fall within the 0.47 – 2.14 $\mu$ m  
3 wavelength range. For wavelengths that are longer than 2.14 $\mu$ m we use the surface emissivity  
4 dataset used in MODIS clear-sky profile retrievals (Seemann et al. 2008). For wavelengths  
5 shorter than 0.47 $\mu$ m we use a seasonally averaged surface albedo database utilized by the  
6 MODIS deep-blue algorithm (Hsu et al. 2004) to obtain the albedo for the 0.41 $\mu$ m channel  
7 and then interpolate for the 0.44  $\mu$ m channel.

8 Over snow and sea ice we use the MODIS zonal snow/ice albedo dataset (Moody et al.  
9 2007). The table lookup is determined by the MODIS pixel latitude, the International  
10 Geosphere–Biosphere Programme (IGBP) ecosystem type and snow/ice fractions from  
11 GEOS-5 FRSNO and FRSEAICE model fields.

12 The resulting surface albedo values are written out to file for each study area so that they  
13 can be referenced later for different simulation scenarios involving same area and time. A  
14 good example of such varying scenarios would be repeated experiments with or without the  
15 presence of aerosols.

## 16 2.2 Water vapor and other gaseous absorbers

17 After the surface albedo calculations are complete, we proceed to ingest the profiles of  
18 temperature, relative humidity, ozone concentration and atmospheric pressure. These profiles  
19 are downsampled to 27 atmospheric levels, as listed in Table 3, from the GEOS-5 native 72  
20 vertical levels and sent to an atmospheric transmittance module that uses the correlated- $k$   
21 method (Kratz, 1995) to calculate weights and optical thicknesses for each atmospheric layer  
22 due to water vapor and other gaseous absorbers. In cases where the surface is encountered at  
23 an altitude higher than 0 km, the profile is trimmed accordingly and the surface level is  
24 inserted as the last level to be used. We perform the vertical downsampling in order to save on



1 the computational cost of the equivalent sensor radiance simulation step, with the bulk of  
2 downsampling occurring above the tropopause. We preserve finer vertical resolution in the  
3 troposphere. We find this to be permissible as radiance data stored in a MODIS L1B file has  
4 an accuracy to only the 5<sup>th</sup> decimal place and the uncertainty due to varying the number of  
5 vertical levels in the upper atmosphere is less than this data storage accuracy.

### 6 2.3 Generating cloud subcolumns

7 Sampling of model cloud-related fields to the MODIS pixel scale is not straightforward  
8 because cloud properties typically vary on scales not adequately resolved by the operational  
9 0.25° GEOS-5 resolution. To sample cloud fields, 1 km MODIS pixels for each GEOS-5  
10 gridcolumn are collected and the same number of pixel-like sub-columns is generated using a  
11 statistical model of sub-gridcolumn moisture variability. The general approach of Norris et al.  
12 (2008) is followed, namely using a parameterized probability density function (PDF) of total  
13 water content for each model layer and a Gaussian copula to correlate these PDFs in the  
14 vertical.

15 In this application, we use the skewed triangle PDF, which allows a simple inclusion of  
16 moisture variability skewness, a ubiquitous feature of atmospheric boundary layers. This PDF  
17 has a simple scalene form characterized by three parameters: a lower and upper bound and a  
18 mode. Under some circumstances, these three parameters can be directly diagnosed from the  
19 *layer mean* total water and condensate contents,  $q_t$  and  $q_c$ , and cloud fraction  $f$ , but in many  
20 cases some adjustments are necessary to  $f$ , and possibly  $q_c$ , to achieve consistency. The details  
21 of this calculation are beyond the scope of this paper and are described fully in Norris and da  
22 Silva (2013). Approximations must also be made in the case of clear or overcast layers, when  
23 the triangle is under-determined.

1        For the Gaussian copula we use a correlation matrix with a fixed vertical decorrelation  
2        scale of 100 hPa, further modified by a multiplicative Riishojgaard (1998) flow-dependent  
3        correlation in total water that permits sharper decorrelation across inversion features. Further  
4        details are given in Norris and da Silva (2013). Once the correlation matrix is specified, the  
5        Gaussian copula correlated ranks of each of the gridcolumn's layers are easily generated  
6        (Norris *et al.*, 2008) and then inverted with the cumulative distribution function (CDF) of  
7        each layer's skewed triangle distribution. The net result is an ensemble of subcolumns of total  
8        moisture content that sample the specified layer PDFs and have the specified vertical  
9        correlations and accompanying cloud and condensate overlap properties. The transformation  
10       of total moisture content to vapor, liquid water and ice contents assumes the vapor is capped  
11       at the GEOS-5 saturation vapor content and that the excess moisture is condensate, split  
12       between the phases using an ice fraction linear in temperature over the -35 to 0°C range. It is  
13       these subcolumn condensates, combined with GEOS-5 diagnostic effective radii, that are used  
14       to evaluate subcolumn (or "pixel") liquid water and ice optical thicknesses for each layer.  
15       These are input to the MODIS radiance simulator code.

16       Note that the subcolumns generated in this way are horizontally independent (the  
17       independent column approximation or ICA), but are subsequently "clumped," or rearranged,  
18       to give horizontal spatial coherence, by using a horizontal Gaussian copula applied to  
19       condensed water path. This clumping acts to give the generated clouds a reasonable horizontal  
20       structure, such that the cloudy pixels in a gridcolumn are actually grouped into reasonable  
21       looking clouds, rather than being randomly distributed. This is important because the MODIS  
22       cloud optical and microphysical properties retrieval algorithm has some spatial variance tests  
23       for potentially partially-cloudy pixels, removing cloud edges by the so-called "clear-sky  
24       restoral" (Zhang and Platnick 2011; Pincus *et al.* 2012). If clumping is not used, then

individual points generated by ICA stand an exceptionally high chance of being eliminated by the clear sky restoral unless a model grid box has a nearly 100% cloud fraction.

In practice, the clumping algorithm works as follows: a correlation matrix  $C$  is a generated between all pixels in a gridcolumn based on the distance between the actual pixels in the MODIS granule and assuming a nominal 5 km decorrelation length. If there are  $N$  pixels,  $C$  is an  $N \times N$  matrix. This matrix is used by a Gaussian copula to generate  $N$  correlated ranks, which are subsequently used to sample (effectively, to re-order) a list of the  $N$  *simulated* pixels that has previously been sorted by column condensed water path (CWP). Because horizontally nearby pixels are more correlated by  $C$ , they will have a higher chance of having similar ranks, and therefore similar values of CWP. In this way the pixels are grouped together horizontally into coherent clouds. [Note that this clumping acts on subcolumns as a whole, and independent of the preexisting vertical correlations in the ICA subcolumns, so the clumping will work better for single cloud layers. For multilayer clouds, the layer that dominates the CWP will dominate the clumping.]

The sub-gridcolumn cloud generator described above is, of course, only one of many possible generators. A less complicated example, very much akin to the internal GEOS-5 treatment of cloud overlap, would be the following “homogeneous cloud, maximum-random overlap” generator: divide the atmosphere into pressure bands, e.g., low, middle and high bands, with interfaces at 700 and 400 hPa. Say we again wish to generate  $N$  subcolumns,  $n = 1, \dots, N$ , for the gridcolumn. Then for each pressure band, generate a set of  $N$  uniform random numbers  $\{r_n\}$  on  $[0,1]$ , and for each model layer  $k$  falling within the band, assign cloudiness to layer  $k$  of subcolumn  $n$  if  $r_n < f_k$ , where  $f_k$  is that layer’s cloud fraction. The fact that the *same* set  $\{r_n\}$  is used for each layer  $k$  in the band enforces maximum cloud overlap *within* the band. But choosing independent sets of  $\{r_n\}$  for each pressure band enforces random overlap

1 *between* the bands. Finally, every subcolumn which is cloudy at layer  $k$ , shares the same  
2 homogeneous in-cloud condensate contents  $\frac{q_{(i,l)k}}{f_k}$ , where  $q_{(i,l)k}$  are the layer mean condensate  
3 contents (i=ice, l=liquid water).

4 Note that this simple generator, as with the earlier more sophisticated generator, produces  
5 subcolumns of *condensate*. The specification of optical thicknesses from condensate contents  
6 proceeds in the same way in both generators, as presented earlier. We emphasize this strategy  
7 because the reader should be very aware of the potential traps associated with using  
8 diagnostic layer cloud optical thicknesses *directly* from GCM (e.g., GEOS-5) output files.  
9 When using diagnostic layer cloud optical thicknesses directly, one must know whether they  
10 are in-cloud or “layer mean”, and if in-cloud, for what cloud fraction. For example, for  
11 GEOS-5, the layer cloud optical thicknesses TAUCLW and TAUCLI are “in-cloud” values  
12 consistent with the maximum cloud fraction  $f_{max}$  of the layer’s pressure band, *not* with the  
13 layer’s actual cloud fraction  $f_k$ . This is because the GEOS-5 diagnostics internally dilute each  
14 layer’s in-cloud cloud optical thickness (in an approximately radiatively-consistent manner)  
15 by stretching each layer’s cloud fraction to its band’s  $f_{max}$ , in order that it may simply add the  
16 diluted layer “in-cloud cloud optical thicknesses” within a band to produce a “band in-cloud  
17 cloud optical depth”, such as GEOS-5’s “TAULOW”. Because of this, the GEOS-5  
18 diagnostic TAULOW, for example, can be regarded as the low-band in-cloud cloud optical  
19 thickness consistent with the model’s low band cloud fraction CLDLOW. Similarly for  
20 TAUMID and TAUHGH. But note that one cannot simply add TAULOW, TAUMID and  
21 TAUHGH to get a column in-cloud optical thickness, because the actual column value  
22 depends on the overlap of these bands. Currently this overlap is random, and so we could  
23 express the column in-cloud optical thickness in terms of the sum over the  $2^3$  combinations of  
24 cloud/clear in the three bands, each with their respective fractions (e.g., a fraction

CLDLOW\*CLDMID\*CLDHGH of the gridcolumn would have a column TAU of  
 TAULOW+TAUMID+TAUHG, a fraction CLDLOW\*CLDMID\*(1-CLDHGH) would  
 have a column TAU of TAULOW+TAUMID, etc.), and finally all normalized by the column  
 cloud fraction CLDTOT = 1 – (1-CLDLOW)\*(1-CLDMID)\*(1-CLDHGH).

Not surprisingly this gives

$$TAUTOT = \frac{CLDLOW * TAULOW + CLDMID * TAUMID + CLDHGH * TAUHG}{CLDTOT}$$

for the column in-cloud optical thickness, because we are assuming that we can average  
 optical thickness (including zeros) in the horizontal, to get a layer mean optical thickness.  
 That assumption in itself is rather questionable, since cloud radiative properties are non-linear  
 in optical thickness. It is therefore much more accurate to deal with radiative averages over  
 subcolumn ensemble optical thicknesses, generated as we have described, than with “layer  
 mean” or “band in-cloud” optical thicknesses directly.

The point we are ultimately making is that one cannot simply interpret the column  
 consequences of model layer cloud diagnostics without a knowledge of the model’s cloud  
 overlap. This is why GEOS-5 now includes the COSP simulator suite to produce satellite  
 observables with an inbuilt treatment of the model overlap.

## 2.4 Radiative transfer calculation

Now that we’ve collected all the necessary information about atmosphere and cloud  
 layers, we begin the simulation process. The radiative transfer calculations were performed  
 using the Discrete Ordinate Radiative Transfer (DISORT) code (Stamnes et al. 1988) with  
 liquid water cloud phase function results from Mie calculations based on gamma distribution  
 water droplet size distributions with an effective variance of 0.1 and bulk ice cloud phase  
 models developed by Baum et al. (2005), both consistent with MOD06. We have

1 experimented with a different number of computational streams in order to balance speed and  
2 desired accuracy. We found that only 16 streams were required to achieve the needed  
3 precision. Generally a large number of streams is required to accurately model the forward  
4 peak of the phase function and multiple scattering components. Initial calculations were done  
5 with 32 streams, however the execution time was rather prohibitive. We settled on 16 streams  
6 as a balance between execution time and precision as the difference in resulting equivalent  
7 sensor radiance between 32 and 16 stream simulations was less than 0.5%.. Also the forward  
8 peak is further truncated and use of the delta-fit method of Hu et al. (2000) can be considered  
9 sufficiently accurate, as described by Ding et al (2009), for calculations where there is no  
10 stored accuracy limit such as the multilayer cloud simulations in Wind et al (2010). As we  
11 pre-calculate the surface spectral albedos, we can save further time by calling DISORT in  
12 Lambertian mode with predetermined values. When we encounter cloud subcolumns over the  
13 ocean, however, we must adjust the computed Cox-Munk surface albedo to compensate for  
14 the diffuse illumination that the presence of the cloud creates. A good value for the diffuse  
15 illumination albedo of a water surface is 0.05 (Platnick et al. 2003). We then linearly fit  
16 surface albedo as a function of cloud optical thickness, with full diffuse illumination at a total  
17 column cloud optical thickness of 3 and full Cox-Munk surface albedo at total column cloud  
18 optical thickness of 0.

19

### 20 **3 Example retrievals**

21 In this section we discuss two example results of radiance simulations and subsequent  
22 cloud property retrievals. We performed the simulation on the NASA Center for Climate  
23 Simulations (NCCS) Discover system using 12 Intel Westmere nodes with 12 cores each. The  
24 memory footprint of the software suite is very small, around 80 Mb peak usage, but the  
25 process is quite CPU-heavy. A full-resolution 1 km simulation using a full MODIS granule as

1 a study area took about three and a half hours wall clock time to complete. Figure 1 shows  
2 resulting true-color RGB image of sample MODIS granule 2012 day 228 (August 15<sup>th</sup>) at  
3 12:00 UTC together with the true-color image of the actual MODIS granule before its channel  
4 data was replaced. Panel a) shows the actual data acquired by Aqua MODIS and panel b)  
5 shows the simulation result. GEOS-5 does not assimilate cloudy radiances and so there should  
6 be little expectation of a granule-level feature match. However, in this case the model does  
7 remarkably well with cloud placement. Bands of cloud over southern France are present and  
8 located properly, as are clouds over the northern Balkans and southern Asia Minor. The  
9 orographic clouds over Italy and Greece are also present, as are scattered clouds over the  
10 Sahara desert. There are some rather important differences between the model and the actual  
11 data, however, when it comes to cloud properties.

12 Figure 2 shows the results of running the Data Collection 5.1 operational retrieval chain  
13 on the resulting L1B file from model fields. Panel a) shows the cloud thermodynamic phase,  
14 panel b) the cloud top pressure, panel c) the cloud optical thickness and panel d) the cloud  
15 effective radius retrieved with the VNSWIR (Visible, Near- or ShortWave InfraRed) and  
16 2.1 $\mu$ m channel combination. Figure 3 shows the actual Aqua MODIS retrieval for that same  
17 granule using identical panel arrangement.

18 The cloud field over the central Mediterranean is given improper vertical location by the  
19 model. The actual cloud field is retrieved as liquid water and is low cloud, with cloud top  
20 pressures of 800-900mb. The model generates a thin cirrus cloud in that location with cloud  
21 top pressure of about 100mb and of course ice thermodynamic phase. This has serious  
22 implications for outgoing radiation. The cloud field over Romania has a consistent phase, but  
23 the model indicates the cloud to be positioned somewhat higher in altitude than the  
24 observation and also significantly optically thicker than what is observed. The same is true for  
25 the cloud field over NW Turkey.

Figure 4 shows a cloud top pressure / cloud optical thickness joint histogram for the actual granule in panel a) and simulated one in panel b). While in this comparison we are not necessarily looking for quantitative evaluation of model parameters, some things do tend to jump out. The actual MODIS granule has mostly low clouds that are moderately thick. The simulated granule on the other hand lacks low clouds almost entirely and instead produces thicker clouds at high altitude. The RGB images look very similar in this case, so the model is performing well on geographical cloud placement, but fails rather badly when it comes to proper cloud placement in altitude. This kind of disconnect can have some significant implications for Earth radiative budget calculations. It is one of our future goals to determine just how frequently such disconnects occur on the global scale.

Figures 5 through 8 show another simulation example, this time from Terra MODIS 2013 day 151 (05.31.2013) at 11:15UTC. Figure 5 shows a true-color RGB image for simulated and actual MODIS granule together with the SWIR composite that allows user to visually estimate cloud thermodynamic phase. Ice clouds appear red in such image. We cannot show a SWIR composite for Aqua MODIS because of detector issues with the Aqua MODIS 1.6 $\mu$ m channel that is needed to create the image. Figure 6 shows retrieval results for the simulated granule, figure 7 shows the actual Terra MODIS granule retrievals. Figure 8 shows the joint histograms of cloud top pressure and cloud optical thickness. In this case there is actually reasonable agreement between sensor measurement and model cloud field representation both geographically and vertically. The model could have benefitted from producing somewhat more mid-level clouds, but overall the large convective system that dominates the scene is represented reasonably well, as are the broken clouds around it. In this case the MODIS operational cloud mask had some trouble detecting clouds in the sun glint region, but sun glint quite often can be a challenging area for retrieval algorithms.

The MODIS cloud top pressure retrieval is quite sensitive to ancillary atmospheric



1 profile information (Menzel et al 2008) and some of differences found in retrievals could be a  
2 result of different representations of the atmospheric profile by GEOS-5 and the NCEP  
3 Mesoscale Meteorological Model (MM5)-derived model profiles used during the MODIS  
4 retrieval.

5 Situations in which cloud optical thickness retrievals show significant differences tend to  
6 be more indicative of significant differences in cloud structure. Unlike cloud top pressure,  
7 cloud optical thickness retrievals have very little dependence on atmospheric profile  
8 information as there is very little atmospheric absorption in the 0.65 and 0.86 $\mu$ m channels  
9 used to retrieve this quantity

10 Cloud effective radius retrievals from the 2.1 $\mu$ m channel depend somewhat on the  
11 atmospheric profile, but differences in that retrieval are also mainly due to differences in  
12 cloud microphysics present in the model and in the actual atmosphere. Retrieved cloud  
13 effective radius appears to be somewhat smaller overall for GEOS-5 data than for MODIS.  
14 Even though the clumped-ICA cloud formation method allows us to model some of the scene  
15 inhomogeneity normally encountered in actual MODIS data, the present implementation of  
16 the simulator does not admit sub-pixel-based effective radius artifacts such as ones appearing  
17 in MODIS (Zhang and Platnick, 2011). Also, GEOS-5 uses a simple diagnostic prescription  
18 of cloud effective radius that is loosely based on large scale observations of aerosol  
19 concentrations and their physical connection to cloud droplet size, and with the details being  
20 adapted based on consistency with surface radiation budget estimates of shortwave cloud  
21 forcing. It is therefore not surprising that, in our preliminary results, there appears to be  
22 generally somewhat less variability in retrieved cloud effective radius from GEOS-5 than  
23 from real MODIS data.

#### 24 **4 Conclusions and future directions**

25 We have developed a flexible software suite that allows us to interface model fields to

1 operational satellite remote sensing retrieval algorithms. We have presented an example of its  
2 operation using the GEOS-5 model and MODIS instrument. We have demonstrated the power  
3 of this software in locating and quantifying problems with GEOS-5 cloud optical properties  
4 and cloud vertical distributions within the specific geographic and synoptic contexts observed  
5 in MODIS cloud granules.

6 In subsequent papers we will show a number of applications of this software. Our current  
7 plans include performing a number of large-scale simulation experiments using GEOS-5  
8 nature run model data with resolutions as high as 7 km. We would like to examine aerosol-  
9 cloud interactions by performing simulations with and without model aerosol fields. Once  
10 operational cloud and aerosol retrieval algorithms are applied to such data, we may be able to  
11 quantify some aerosol effects on clouds and maybe even find some ways to retrieve aerosols  
12 above clouds.

13 We would also like to examine in detail the performance of COSP, the Cloud Feedback  
14 Model Intercomparison Project (CFMIP) Observation Simulator Package, which provides a  
15 means of simulating retrieved cloud properties from a variety of instruments, including  
16 MODIS, from model fields. The COSP package typically uses approximate, so-called “fast”  
17 simulators of cloud properties, whereas we are directly simulating radiances and performing  
18 the retrievals using actual operational retrieval codes. We thus have the ability to test the  
19 quality of the COSP fast simulators

20 We also intend to apply this software suite to other remote sensing instruments, such as  
21 SEVIRI (Spinning Enhanced Visible Infrared Radiometer Imager) onboard the Meteosat  
22 Second Generation geostationary satellite series. SEVIRI has a sufficient number of channels  
23 that MODIS-style cloud retrieval algorithms can be applied. SEVIRI acquires data in 15  
24 minute intervals at 3 km nadir resolution, thus giving fine temporal and spatial resolution for  
25 diurnal sampling. Applying the equivalent sensor radiance package to SEVIRI would allow us

1 potentially to examine model cloud dynamics at a temporal resolution not offered by polar  
2 orbiting satellites.

3 We are confident that there are many other applications for this software that will be  
4 found in the future besides ones outlined above and that it will become a valuable tool for  
5 both the remote sensing and modeling communities.

6 The simulator code is available to users free of charge by contacting the authors and  
7 becoming a registered user of this software package so that any updates can be issued directly.  
8 There may be additional, wider distribution means in the future if the software shows signs of  
9 growing popularity.

## 10 **Acknowledgements**

11 The authors would like to thank the MODAPS members Georgios Britzolakis, Kurt  
12 Hoffman and Gang Ye for assisting us in processing simulated radiance files through the  
13 operational retrieval algorithm chain.

## References

- Ackerman, A., K. Strabala, P. Menzel, R. Frey, C. Moeller, L. Gumley, B. Baum, S. W. Seemann, and H. Zhang, 2006: Discriminating clear-sky from cloud with MODIS Algorithm Theoretical Basis Document (MOD35). ATBD Reference Number: ATBD-MOD-06. [http://modis-atmos.gsfc.nasa.gov/reference\\_atbd.html](http://modis-atmos.gsfc.nasa.gov/reference_atbd.html)
- Barnes, W. L., T. S. Pagano, and V. V. Salomonson, 1998: Prelaunch characteristics of the Moderate Resolution Imaging Spectroradiometer (MODIS) on EOS-AM1. *IEEE Trans. Geosci. Remote Sens.*, 36, 088–1100.
- Bony, S., R. Colman, V. M. Kattsov, R. P. Allan, C. S. Bretherton, J. L. Dufresne, A. Hall, S. Hallegatte, M. M. Holland, W. Ingram, D. A. Randall, B. J. Soden, G. Tselioudis and M. J. Webb, 2006: How well do we understand and evaluate climate change feedback processes?, *J. Climate*, 19, 3445–3482.
- Baum, B.A, A. J. Heymsfield, P. Yang, and S. T. Bedka, 2005a: Bulk scattering models for the remote sensing of ice clouds. Part 1: Microphysical data and models. *J. Appl. Meteor.*, 44, 1885–1895.
- Colarco, P., A. da Silva, M. Chin, T. Diehl, 2010: Online simulations of global aerosol distributions in the NASA GEOS-4 model and comparisons to satellite and ground-based aerosol optical depth. *J. Geophys. Res.*, 115, D14207, doi:10.1029/2009JD012820
- Cox, C., W. Munk, 1954: Measurement of the Roughness of the Sea Surface from Photographs of the Sun's Glitter. *J. Opt. Soc. Am.*, 44, 838–850
- Derber, J. C., R. J. Purser, W.-S. Wu, R. Treadon, M. Pondeva, D. Parrish, and D. Kleist, 2003: Flow-dependent Jb in a global grid-point 3D-Var. *Proc. ECMWF annual seminar on recent developments in data assimilation for atmosphere and ocean*. Reading, UK, 8–12 Sept. 2003.
- Ding, S., Y. Xie, P. Yang, F. Weng, Q. Liu, B. Baum, and Y. Hu, 2009: Estimates of radiation over clouds and dust aerosols: Optimized number of terms in phase function expansion. *J. Quant. Spectrosc. Radiat. Transfer*, 110, 1190–1198.
- Feldman, D. R., C. A. Algeri, J. R. Ong, W. D. Collins, 2011: CLARREO shortwave observing system simulation experiments of the twenty-first century: Simulator design and implementation. *J. Geophys. Res.*, 116, D10107, doi: 10.1029/2010JD015350

1 Frey, R. A., S. A. Ackerman, Y. Liu, K. I. Strabala, H. Zhang, J. Key and X. Wang, 2008:  
2 Cloud Detection with MODIS, Part I: Recent Improvements in the MODIS Cloud Mask,  
3 JTECH 25, 1057-1072.

4 Hill, C., C. DeLuca, V. Balaji, M. Suarez, A. da Silva, 2004: The architecture of the Earth  
5 System Modeling Framework, *Comp. Sci. Engr.*, 6(1), 18-28.

6 Hsu, N.C., S. Tsay, M.D. King and J.R. Herman, 2004: Aerosol Properties Over Bright-  
7 Reflecting Source Regions. *IEEE Trans. Geosci. Rem. Sens.*, 42, 557-569

8 Hu, Y.-X., B. Wielicki, B. Lin, G. Gibson, S.-C. Tsay, K. Stamnes, and T. Wong, 2000: d-Fit:  
9 A fast and accurate treatment of particle scattering phase functions with weighted singular-  
10 value decomposition least-squares fitting. *J. Quant. Spectrosc. Radiat. Transfer*, 65, 681–  
11 690.

12 Hubanks, P. A, M. D. King, S. A. Platnick, and R. A. Pincus, 2008: MODIS Atmosphere L3  
13 Gridded Product Algorithm Theoretical Basis Document. ATBD Reference Number:  
14 ATBD-MOD-30. [http://modis-atmos.gsfc.nasa.gov/MOD08\\_M3/atbd.html](http://modis-atmos.gsfc.nasa.gov/MOD08_M3/atbd.html)

15 Intergovernmental Panel on Climate Change (IPCC), 2007: Climate Change 2007: The  
16 Physical Science Basis. Contribution of Working Group I to the Fourth Assessment  
17 Report of the Intergovernmental Panel on Climate Change, edited by S. Solomon et al.  
18 Cambridge Univ. Press, Cambridge, UK

19 King, M. D., W. P. Menzel, Y. J. Kaufman, D. Tanré, B. C. Gao, S. Platnick, S. A. Ackerman,  
20 L. A. Remer, R. Pincus, and P. A. Hubanks, 2003: Cloud and aerosol properties,  
21 precipitable water, and profiles of temperature and humidity from MODIS. *IEEE Trans.*  
22 *Geosci. Remote Sens.*, 41, 442–458.

23 King, M. D., S. Platnick, W. P. Menzel, S. A. Ackerman, and P. A. Hubanks: Spatial and Temporal  
24 Distribution of Clouds Observed by MODIS onboard the Terra and Aqua Satellites, *IEEE Trans.*  
25 *Geosci. Remote Sens.* (submitted April 2012, revised Aug 2012, accepted Oct. 28, scheduled to  
26 appear in print July 2013).

27 Kratz, D. P., 1995: The correlated k-distribution technique as applied to the AVHRR  
28 channels. *J. Quant. Spectrosc. Radiat. Transfer*, 53, 501–517.

29 Menzel, W. P., R. Frey, H. Zhang, D. Wylie, C. Moeller, R. Holz, B. Maddux, B. A. Baum,  
30 K. Strabala, and L. Gumley, 2008: MODIS global cloud-top pressure and amount  
31 estimation: Algorithm description and results. *J. Appl. Meteor. Climatol.*, 47, 1175–1198.

1 Molod, A., L. Takacs, M. Suarez, J. Bacmeister, I.-S. Song, and A. Eichmann, 2012: The  
2 GEOS-5 Atmospheric General Circulation Model: Mean Climate and Development from  
3 MERRA to Fortuna. Tech. Rep. S. Gl. Mod. Data Assim., 28

4 Moody, E. G., M. D. King, S. Platnick, C. B. Schaaf, and F. Gao, 2005: Spatially complete  
5 global spectral surface albedos: Value-added datasets derived from Terra MODIS land  
6 products. *IEEE Trans. Geosci. Remote Sens.*, 43, 144–158.

7 Moody, E. G., M. D. King, C. B. Schaaf, D. K. Hall, and S. Platnick, 2007: Northern  
8 Hemisphere five-year average (2000-2004) spectral albedos of surfaces in the presence of  
9 snow: Statistics computed from Terra MODIS land products. *Remote Sens. Environ.*, 111,  
10 337–345.

11 Moody, E. G., M. D. King, C. B. Schaaf and S. Platnick, 2008: MODIS-derived spatially  
12 complete surface albedo products: Spatial and temporal pixel distribution and zonal  
13 averages. *J. Appl. Meteor. Climatol.*, 47, 2879–2894.

14 Norris, P. M., L. Oreopoulos, A. Y. Hou, W.-K. Tao, X. Zeng, 2008: Representation of 3D  
15 heterogeneous cloud fields using copulas: Theory for water clouds. *J. Q. R. Meteorol. Soc.*  
16 134: 1843–1864. doi:10.1002/qj.321.

17 Norris, P. M. and A. M. da Silva, 2013: Monte Carlo Bayesian inference on a statistical model  
18 of sub-gridcolumn moisture variability using high-resolution cloud observations. Part I:  
19 Method. Submitted to *J. Q. R. Meteorol. Soc.*

20 Pawson, S. R., S. Stolarski, A. R. Douglass, P. A. Newman, J. E. Nielsen, S. M. Frith, M. L.  
21 Gupta, 2008: Goddard Earth Observing System chemistry-climate model simulations of  
22 stratospheric ozone-temperature coupling between 1950 and 2005, *J. Geophys. Res.* 113,  
23 D12103, doi:10.1029/2007JD009511

24 Platnick, S., M. D. King, S. A. Ackerman, W. P. Menzel, B. A. Baum, J. C. Riedi, and R. A.  
25 Frey, 2003: The MODIS cloud products: Algorithms and examples from Terra. *IEEE*  
26 *Trans. Geosci. Remote Sens.*, 41, 459–473.

27 Rienecker, M.M., M. J. Suarez, R. Todling, J. Bacmeister, L. Takacs, H.-C. Liu, W. Gu, M.  
28 Sienkiewicz, R. D. Koster, R. Gelaro, I. Stajner, and J. E. Nielsen, 2008: The GEOS-5 Data  
29 Assimilation System - Documentation of Versions 5.0.1, 5.1.0, and 5.2.0. Tech. Rep. S. Gl.  
30 Mod. Data Assim., 27

1 Riishojgaard, LP. 1998: A direct way of specifying flow-dependent background error  
2 correlations for meteorological analysis systems. *Tellus* 50A: 42–57.

3 Roberts, Y. L., P. Pilewskie, B. C. Kindel, D. R. Feldman, W. D. Collins 2013: Quantitative  
4 comparison of the variability in observed and simulated shortwave reflectance. *Atmos.*  
5 *Chem. Phys.* 13, 3133-3147

6 Seemann, S. W., E. E. Borbas, R. O. Knuteson, G. R. Stephenson, H-L. Huang, 2008:  
7 Development of a Global Infrared Land Surface Emissivity Database for Application to  
8 Clear Sky Sounding Retrievals from Multispectral Satellite Radiance Measurements. *J.*  
9 *Appl. Meteor. Climatol.*, 47, 108-123.

10 Stamnes, K., S. C. Tsay, W. Wiscombe, and K. Jayaweera, 1988: Numerically stable  
11 algorithm for discrete-ordinate-method radiative transfer in multiple scattering and  
12 emitting layered media. *Appl. Opt.* 27, 2502–2509.

13 Wind, G., S. Platnick, M.D. King, P.A. Hubanks, M.J. Pavolonis, A.K. Heidinger, P. Yang, B.  
14 Baum, 2010: Multilayer Cloud Detection with the MODIS Near-Infrared Water Vapor  
15 Absorption Band. *J. App. Met. Clim.* 49, 2315-2333

16 Wu, W. S., R. J. Purser, D. F. Parrish, 2002: Three-dimensional variational analysis with  
17 spatially inhomogeneous covariances. *Mon. Wea. Rev.*, 130, 2905-2916

18 Xiong, X., A. T. Isaacman, and W. Barnes, 2006: MODIS Level-1B Products. *Earth Science*  
19 *Satellite Remote Sensing, Science and Instruments*, vol 1, 33-49

20 Zhang, Z., and S. Platnick, 2011: An assessment of differences between cloud effective  
21 particle radius for marine water clouds from three MODIS spectral bands. *J. Geophys.*  
22 *Res.*, 116, D20215, doi:10.1029/2011JD016216.

23

1 Table 1. GEOS v.5.7.2 fields and products used in simulations

Field Code	Description
U10M	U-component of wind speed at 10m altitude
V10M	V-component of wind speed at 10m altitude
FRSEAICE	Sea ice fraction
FRSNO	Snow fraction
PS	Surface pressure
T2M	Temperature at 2m altitude
SLP	Mean sea-level pressure
QV2M	Specific humidity at 2m altitude
O3	Ozone concentration profile
T	Temperature profile
DELP	Level pressure differential profile
RH	Relative humidity profile
CLOUD	Radiative cloud fraction profile
QLLS	Large scale cloud liquid water mixing ratio
QLAN	Anvil cloud liquid water mixing ratio
QILS	Large scale cloud ice mixing ratio
QIAN	Anvil cloud ice mixing ratio

2

3



1 Table 2. MODIS channels used in simulations

Channel number	Central wavelength (μm)
1	0.65
2	0.86
3	0.47
4	0.55
5	1.24
6	1.63
7	2.13
8	0.41
9	0.44
17	0.91
18	0.94
19	0.94
20	3.7
22	3.9
26	1.38
27	6.2
28	7.3
29	8.5
31	11.0
32	12.0
33	13.2
34	13.4
35	13.8
36	14.2

2

3

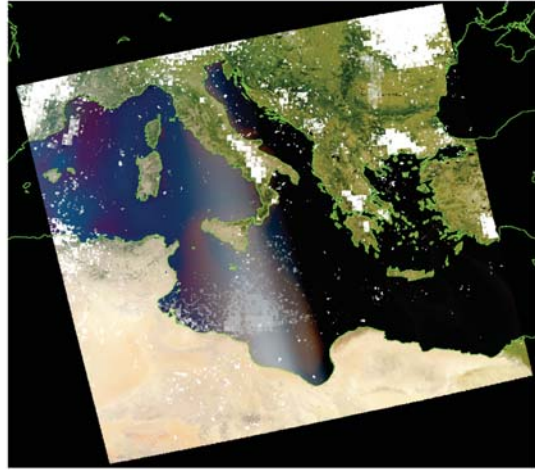
1 Table 3. Vertical levels used in simulation

Level number	Level altitude (km)
1	80
2	60
3	50
4	45
5	40
6	35
7	30
8	25
9	20
10	18
11	16
12	15
13	14
14	13
15	12
16	11
17	10
18	9
19	8
20	7
21	6
22	5
23	4
24	3
25	2
26	1
27	0

a) Actual RGB composite



b) Simulated RGB composite



1

2 Figure 1. Equivalent sensor radiance simulation together with an actual MODIS granule that  
3 was used as study area. Aqua MODIS granule 2012 day 228 at 12:00 UTC. GEOS-5 temporal  
4 fit between 12Z and 18Z 2012.08.15. RGB (0.67 $\mu\text{m}$ , 0.55 $\mu\text{m}$ , 0.47 $\mu\text{m}$ )

5

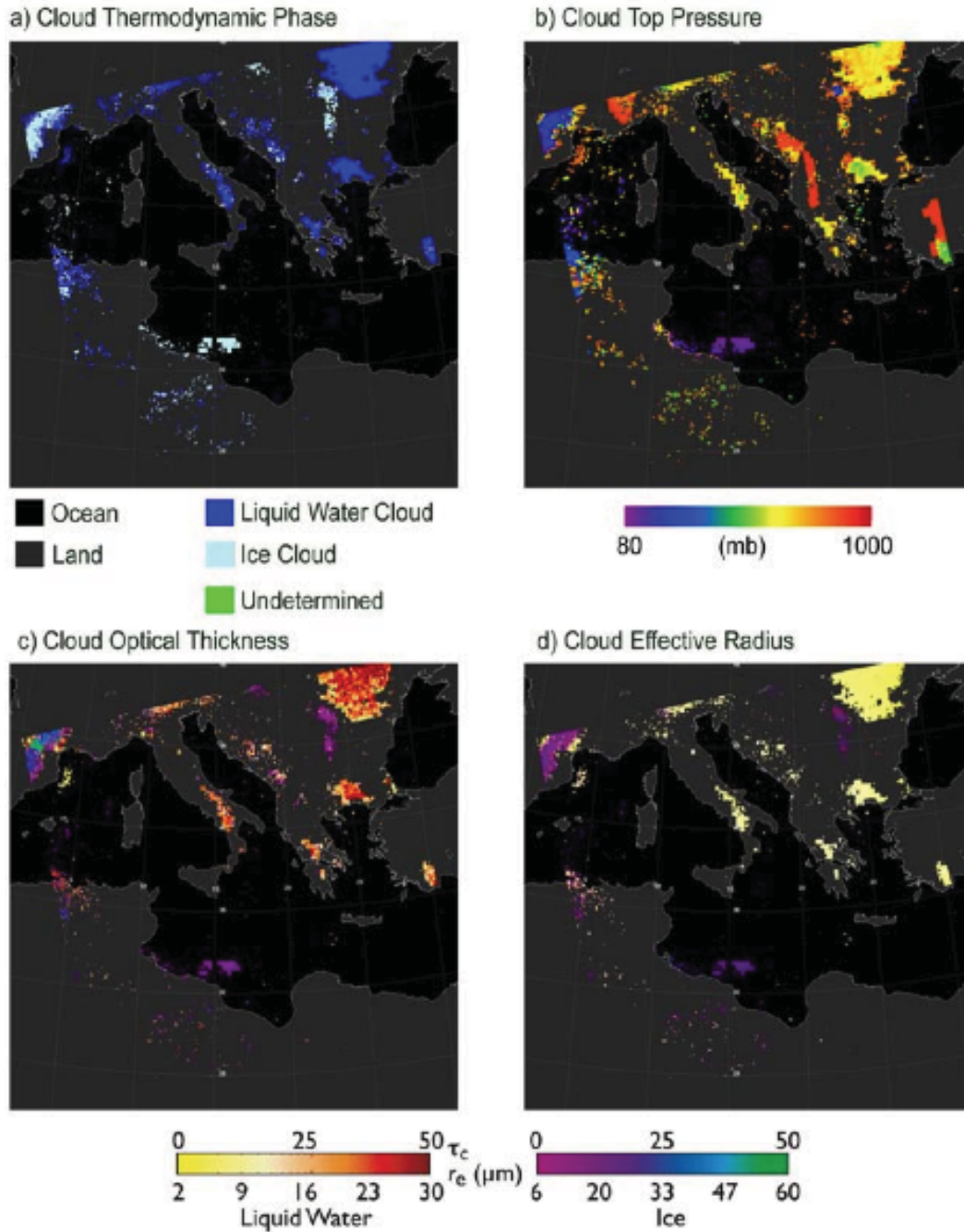


Figure 2. Example cloud retrieval for simulated granule covered by Aqua MODIS 2012 day 288 12:00 UTC. Panel a) is cloud thermodynamic phase, panel b) is cloud top pressure, panel c) is cloud optical thickness and panel d) is cloud effective radius from the 0.86-2.1 $\mu\text{m}$  band combination

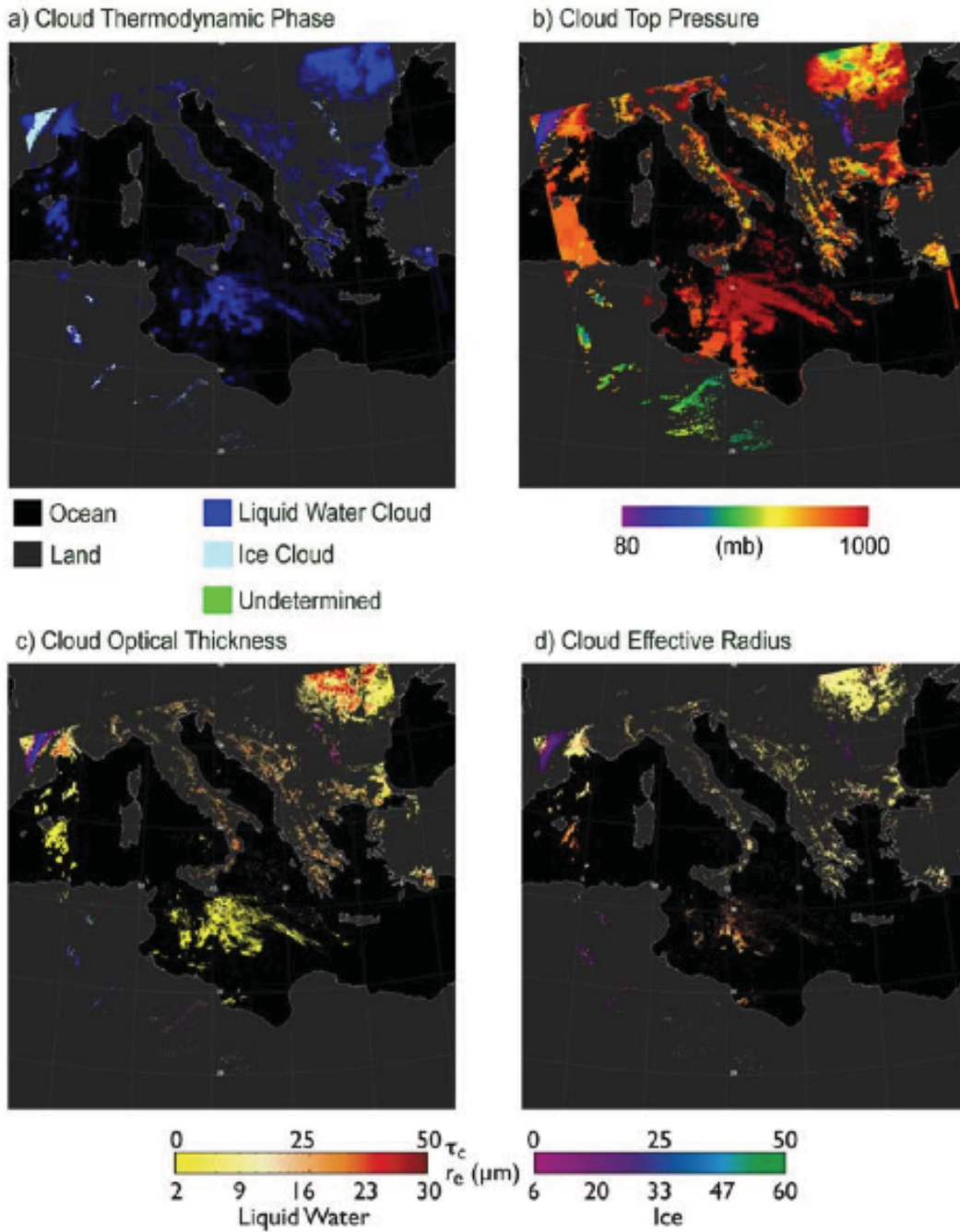


Figure 3. Actual cloud retrieval for Aqua MODIS 2012 day 228 at 12:00 UTC . Panel a) is cloud thermodynamic phase, panel b) is cloud top pressure, panel c) is cloud optical thickness and panel d) is cloud effective radius from the 0.86-2.1 $\mu\text{m}$  band combination.

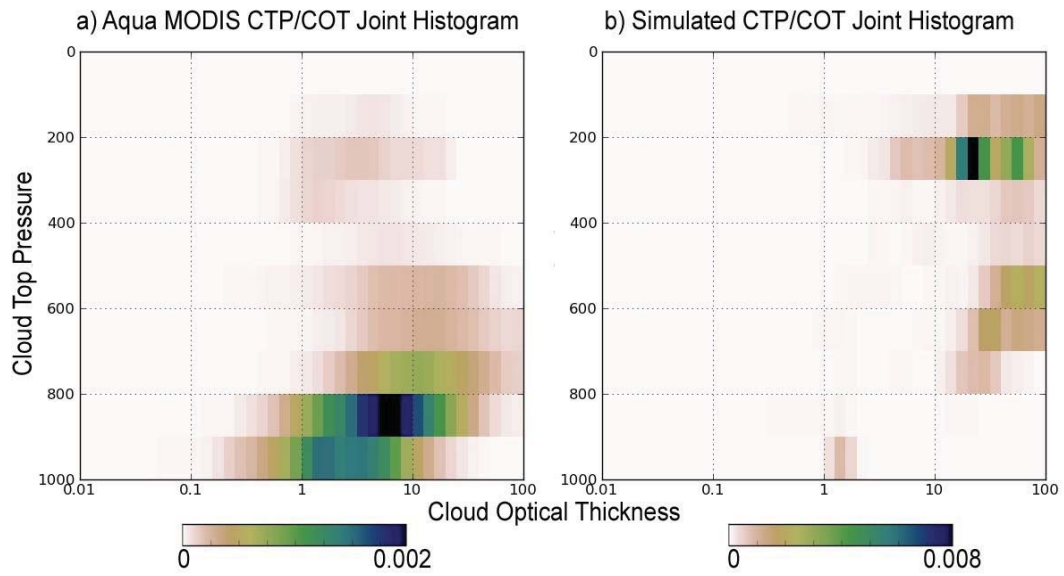
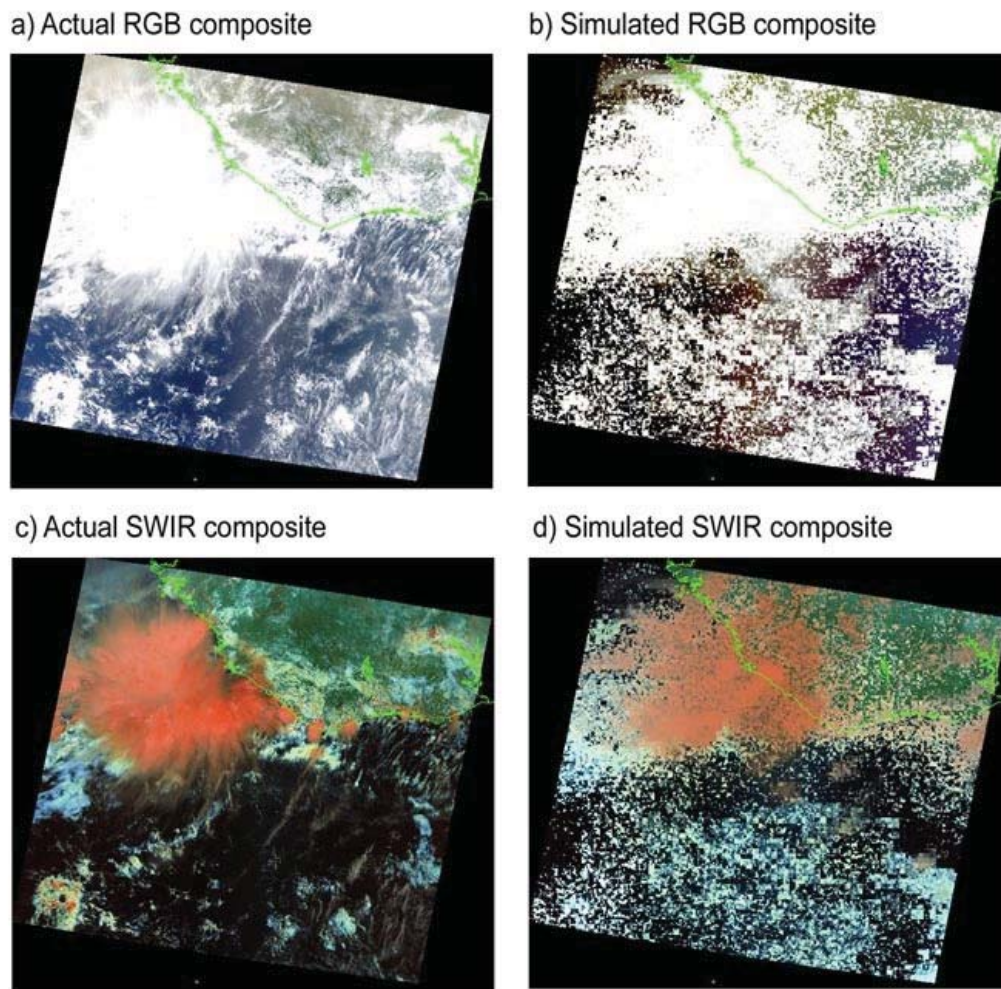


Figure 4. Joint histograms of cloud optical thickness vs cloud top pressure for actual (a) and model-based (b) cloud fields covered by Aqua MODIS 2012 day 228 at 12:00 UTC.



1



2

3 Figure 5. Equivalent sensor radiance simulation together with an actual MODIS granule that  
4 was used as study area. Terra MODIS granule 2013 day 151 at 11:15 UTC. GEOS-5 temporal  
5 fit between 06Z and 12Z 2013.05.31. RGB ( $0.67\mu\text{m}$ ,  $0.55\mu\text{m}$ ,  $0.47\mu\text{m}$ ), SWIR( $0.86\mu\text{m}$ ,  
6  $1.6\mu\text{m}$ ,  $2.1\mu\text{m}$ )

7

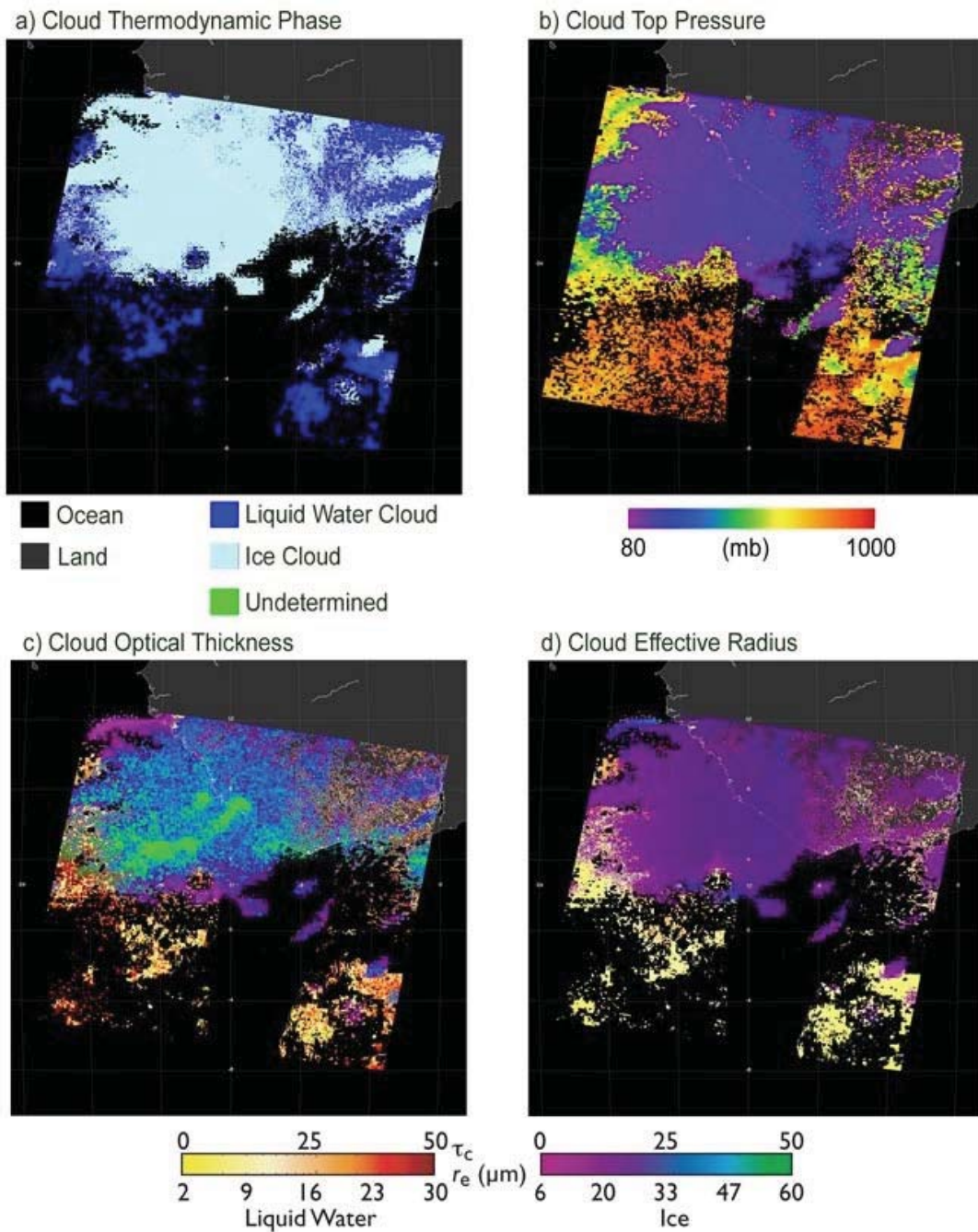


Figure 6. Example cloud retrieval for simulated granule covered by Terra MODIS 2013 day 151 11:15 UTC. Panel a) is cloud thermodynamic phase, panel b) is cloud top pressure, panel c) is cloud optical thickness and panel d) is cloud effective radius from the 0.86-2.1 $\mu\text{m}$  band combination



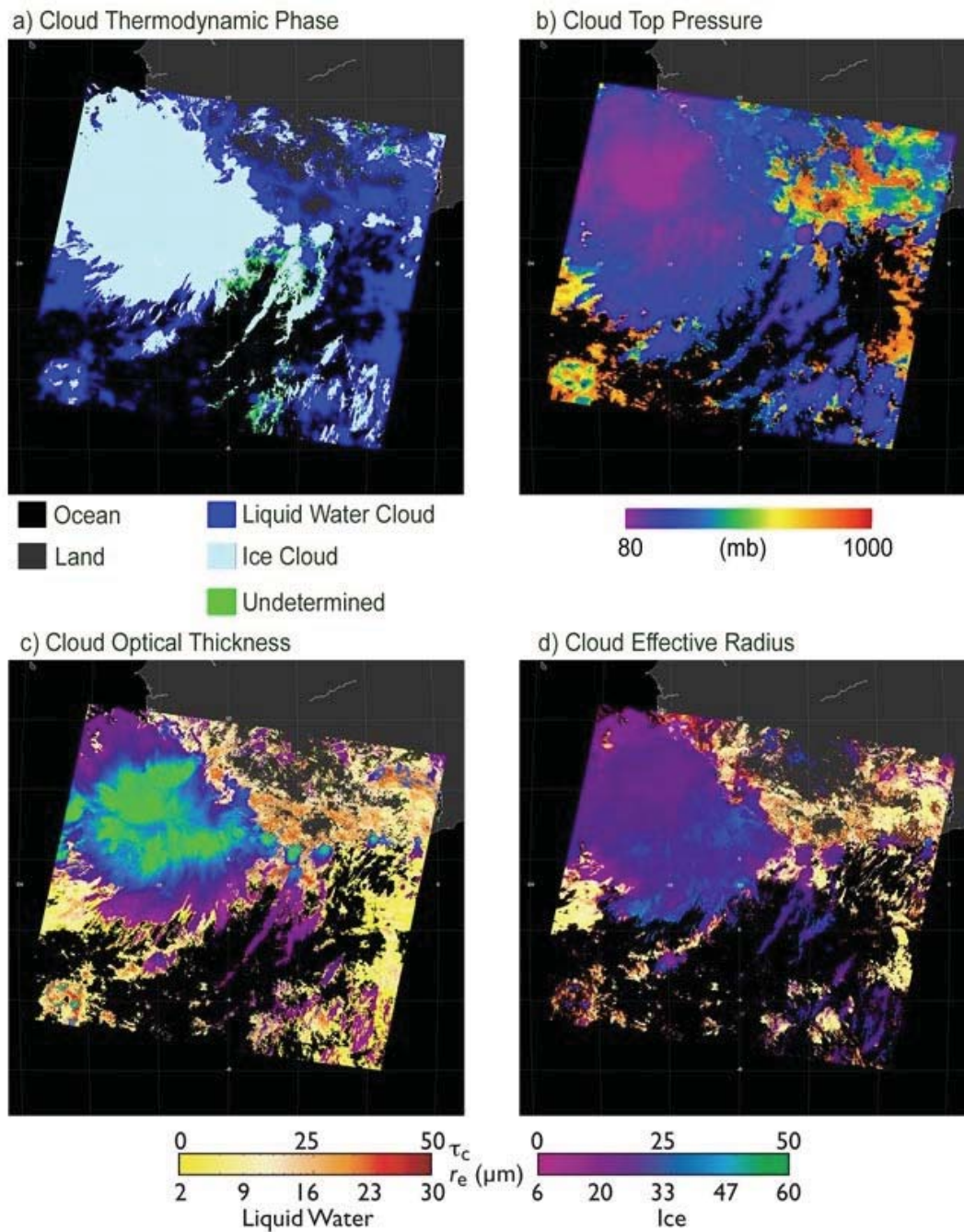


Figure 7. Actual cloud retrieval for Terra MODIS 2013 day 151 at 11:15 UTC . Panel a) is cloud thermodynamic phase, panel b) is cloud top pressure, panel c) is cloud optical thickness and panel d) is cloud effective radius from the 0.86-2.1 $\mu\text{m}$  band combination.

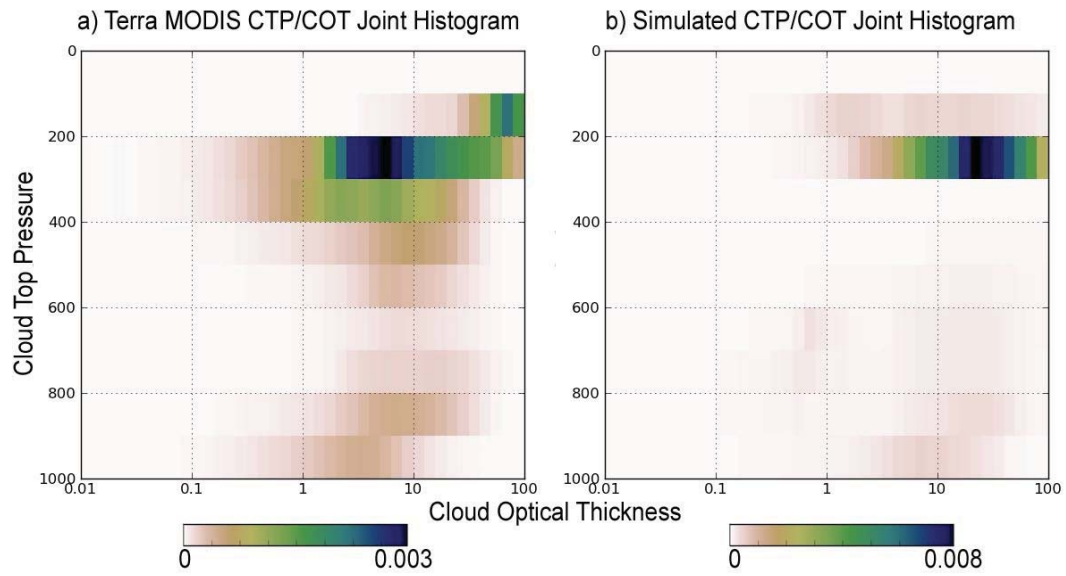


Figure 8. Joint histograms of cloud optical thickness vs cloud top pressure for actual (a) and model-based (b) cloud fields covered by Terra MODIS 2013 day 151 at 11:15 UTC.